The impact of the addition of Bi_2Te_3 nanoparticles on the structural and the magnetic properties of the Bi-2223 high-T_c superconductor.

M.S. Shalaby[1,*], Mai Hussein Hamed[2,3], N.M. Yousif[1], H.M. Hashem[3],

[1,*](Mustafa Shalaby),Dr.,
Solid-State Physics and Accelerators Department, National Center for Radiation Research and Technology, Egyptian Atomic Energy Authority, B.O. Box 29 Nasr City, Cairo, Egypt.
E-mail:phymshalaby@gmail.com, Tel:+2 01112289938,
ORCID: 0000-0002-5634-182x

[2,3] Mai Hussein Hamed, Dr.,
[2]Jülich Centre for Neutron Science JCNS2, Forschungszentrum Jülich GmbH, Jülich 52425, Germany.
[3] Physics Department, Faculty of Science, Helwan University, 11798 Helwan- Cairo, Egypt.
E-mail: maioush1@yahoo.com
ORCID: 0000-0001-8165-1216

[1]NashwaYousif ,Dr.,
Solid-State Physics and Accelerators Department, National Center for Radiation Research and Technology, Egyptian Atomic Energy
Authority, B.O. Box 29 Nasr City, Cairo, Egypt.
E-mail: yousif_nashwa@yahoo.com
ORCID: 0000-0001-6545-9523

[3]Hany Hashem, Dr.,
Physics Department, Faculty of Science, Helwan University, 11798 Helwan- Cairo, Egypt.
E-mail:hany_m_hashem@yahoo.com, Tel:+2 01096743169,
ORCID: 0000-0002-8629-2221

Abstract:

The polycrystalline granular BSCCO high T_c superconductors (HTSC) have limitations in various applications. These limitations appear due to the flux pinning's weakness and the weak links between the grains comparatively in high temperatures and high applied magnetic fields.Bi_2Te_3 nanoparticles are artificially introduced into the Bi-2223 HTCS matrix to be employed as effective flux pinning centers to enhance the flux pinning capability and the critical current density. The effect of the additive of Bi_2Te_3 nanoparticles on the structural and physical properties of Bi-2223 were investigated for the polycrystalline $(Bi_{1.6}Pb_{0.4}Sr_2Ca_2Cu_3O_{10+\delta})_{1-x}/(Bi_2Te_3)_x$ where (x = 0.00,0.01,0.02& 0.03). The phase structure/formation, volume fraction, the lattice constants were described by X-ray powder diffraction (XRD) measurements. Diamagnetic signal has been investigated with two onset temperatures (T_{c1}&T_{c2}) for the common BSCCO phases (Bi-2223 and Bi-2212) which confirm the XRD obtained data without any indication for unwanted impurities. The magnetic interactions between Bi_2Te_3 nanoparticles addition and the superconductor matrix are discussed at 5 and 50 K. The relation between the microstructure, BSCCO phase's contents, the hysteresis loops, the calculated critical current densities, and the flux densities were also reported for the samples. Nano-Bi_2Te_3 shows a great impact on the BSCCO superconducting properties and influences its flux densities and the flux pinning mechanisms as reported experimentally and theoretically. Consequently, the additive of Bi_2Te_3 nanoparticles must be carefully controlled to balance the microstructure and superconducting parameters of the BSCCO HTSC.

Keywords: Powders: solid state reaction, Microstructure-prefiring, Oxide superconductors, Electron microscopy, Magnetic properties, Flux pinning and critical currents density.

1- Introductions

Since the discovery of high oxide superconductors [1,2], Bi-based high-temperature superconductors (HTSC) are one of the significant compounds of Cuprates families. Because of their higher Transition temperature (T_c=110 K) for Bi-2223 phase, favorable mechanical properties, high upper critical magnetic fields H_{c2}, large critical current J_c, BSCCO systems are used widely in a lot of commercial applications such as cables [3–5], magnets [6], magnetic resonance imaging systems (MRI) [7], superconducting fault current limiters (SFCL) [8], and magnetic sensors [9,10]. The superconducting characteristics of the Bi-2223 mechanism are closely associated with its hole concentrations, its pinning ability, and its phase microstructure [11-14]. Therefore, the research interest in the BSCCO systems is concentrated mainly on improving the overall properties of the Bi-2223 phase in order to improve materials properties for practical applications. (J_c) values differ significantly from sample to sample, representing the conditions of preparation and the effect of doping rates. Among the calcined polycrystalline oxide superconductors, it is well known that (J_c) is influenced by the weak-linked aspect of its grain boundary [15, 16].

The method of additions and substitutions is also used to solve the limitations of the Jc and better understand the factors that affect the significant superconducting parameters. It is pointed that the doping level of different types of atoms at distinct positions in HTSC produces a level of crystal defects inside the material. Including the lattice strains' effectiveness, non-superconductive phase inclusions, and other structural inhomogeneities could serve as efficient flux pinning in such a material, increasing critical current density (J_c) in both zeroes as well as the applied fields [17-20].

3d magnetic elements (Co,Zn,Fe …etc) were favorable to be substituted into Cu site in CuO planes because they are close in their ionic size [21-24].This magnetic substitutions suppress the T_c and also affected the J_c values [25, 26]. The magnetic characteristics of doping and the repression of superconducting behaviour are attributed to the solely local disorder produced by the doping concentration. On the other hand, critical temperature T_c and microstructure have been degraded with the rare earth additive in these systems [27]. Where, the doping of Nd [28] and Pr[29] have, conversely, been shown to improve the flux pinning properties of the Bi-2223 HTSC.

Many research studies consider the limitations of the weak links and weak flux pinning capability for the Bi-2223 phase to be used widely in many applications [30]. Generally,

the additive of nanoparticles such as nano-oxides to (Bi,Pb)-2223 superconducting phase participates in enhancing the flux pinning and critical current density [31,32]. Polycrystalline (Bi,Pb)-2223 high T_c superconductor systems were fabricated by solid state reaction technique in the air with (0-0.2% wt) additive from Al_2O_3 nanoparticles [33]. Ghattas et al. found that the critical current density J_c, volume pinning force density, the onset transition temperature T_c and the effective energy U have been enhanced with 0.2% Al_2O_3 additions [34]. Baqiah. et al. synthesized Bi-2223 system by using solid-state reaction method by adding Sm_2O_3 nanoparticles (x=0.00-0.05). The introduction of Sm_2O_3 nanoparticles influenced Bi-2223/Bi-2212 volume fraction ratio and strengthened the Bi-2212 phase formation by x=0-0.02 wt % samples [35].

Jannah and his co workers improve Bi-2223 phase formation by Co_3O_4 addition with different weight % (x=0.0-0.05). They used solid-state reaction method to produce the materials. They achieved the highest T_c =102K, the highest Bi-2223 volume fraction at x= 0.01 % whereas the highest critical current density J_c was observed for x= 0.03% [36]. Other researchers reported the addition of ZrO_2 [37], SiC [38], MgO [39] , Fe_2O_3 [40], MgB_2[41], Nb_2O_5 [42],Cr_2O_3 and FeS [43] nanoparticles that cause different effects on Bi-2223 properties such as the microstructure, the flux pinning and the current density J_c of this system. Careful control of the particle size as well as the doping amount to be held less than the critical level may provide the flux pinning in Bi-2223 HTCS. Moreover, the flux pinning and the other mechanisms are needed for more identifications and studies. Some studies consider the doping of nano-sized magnetic particles that introduce normal-like defects into the superconducting matrix, interact with the vortices, and act as effective pinning centers inside Bi-2223 HTSC [42,44, 45].

In this communication, the additive of topological insulator (Bi_2Te_3) nanoparticles to BSCCO HTSC was investigated for the first time. So the objectives of this study were to determine the consequence of Bi_2Te_3 nanoparticles addition before the final steps of heat treatment of $Bi_{1.6}Pb_{0.4}Sr_2Ca_2Cu_3O_{10+\delta}$ superconductor. The structure, the phase formation, the sample morphology, the magnetic properties, and the critical current density of the samples were discussed in detail.

2-Experimental:

2.1. Samples preparation

Bi_2Te_3 was prepared by the solvothermal technique as mentioned in our previous work [46]. Bi_2Te_3 was grinded for 2 hr by ball milling machine to increase the reduction

of grains sizes. For $(Bi_{1.6}Pb_{0.4}Sr_2Ca_2Cu_3O_{10+\delta})_{1-x}$ $(Bi_2Te_3)_x$ (x = 0.0, 0.01, 0.02, 0.03) composition were synthesized by solid-state reaction technique by appropriate stoichiometric oxides. High-purity powders of Bi_2O_3, $SrCO_3$, CaO, PbO and CuO were used in the preparation process. The Oxides were used to prepare $Bi_{1.6}Pb_{0.4}Sr_2Ca_2Cu_3O_{10+\delta}$ first by grinding the oxides very well for 1 hr in a ball milling machine till the homogeneity was achieved. The initial product was pre-calcinated for 24 hrs at 860˚C, and then it left to cool gradually. It was remarked that the powder turns to dark color. Then, the dark powder was grinded again for 1 hr in the ball milling machine, pressed into discs and sintered for 48 hrs at 870˚C.The final stage is the additive of the Bi_2Te_3 nanoparticles to the powder. the calcinated powder was ground, divided into four parts, and appropriate amounts of Bi_2Te_3 nanoparticles were added with the composition $(Bi_{1.6}Pb_{0.4}Sr_2Ca_2Cu_3O_{10+\delta})_{1-x}$ $(Bi_2Te_3)_x$ (x = 0.0, 0.01, 0.02, 0.03). Each sample was thoroughly mixed and ground for 2 hrs into the ball milling machine with the stoichiometric ratios for each concentration and pressed in a disc-shaped pellet, then sintered for 48 hrs at 850˚C in air.

The powder and Bi_2Te_3 nanoparticles were grinded for 2 hrs into the ball milling machine with the stoichiometric ratios for each concentrations. $(Bi_{1.6}Pb_{0.4}Sr_2Ca_2Cu_3O_{10+\delta})_{1-x}$ $(Bi_2Te_3)_x$ (x = 0.0, 0.01, 0.02, 0.03) output yields from the ball milling were pressed into pellets and sintered for 48 hrs at 850˚C.

2.2. Phase identification

The structural characterization such as the phase identification, unit cell volumes, grain sizes, and the other microstructure investigation were accomplished by employing a completely computerized X-ray diffractometer, Shimadzu XRD-6000 type with CuK_α radiation source (λ=1.54 Å).

Energy-dispersive X-ray spectrometer (EDX) JOEL (JCM-6000PLUS) benchtop scanning electron microscopy (SEM) was employed to examine and determine the elemental composition of the obtained samples. Also, SEM has been used to scan the surface topography of specimens by using ZEISS which deliver high-resolution imaging and superior material contrast.

High-resolution transmission electron microscopy (HRTEM) images were obtained were prepared by dispersing the materials in methanol for 15 min; on the TEM grid film, a drop from the dispersed materials put on it and left to dry. Then the grid was taken and handled into the machine from type (HRTEM, Jem-2100, Jeol, Japan). The negatives of

the micrographs obtained were converted into digital image files with a CCD camera. Computerized image processing, including careful filtering to improve image quality, was performed with the help of image processing software.

2.3. Superconducting measurements.

Magnetization M(T) has been carried out by a vibrating sample magnetometer (VSM) using a Quantum Design Dynacool physical properties measurement system (PPMS). This technique is used for finding out the superconducting signal (Meissner signal) via the investigations of the onset temperature (T_c). These measurements were accomplished at low temperature for two modes; the zero field cooled (ZFC) and field cooled (FC) to stand up on the temperature dependence of the remnant magnetization, M(T). Also, the hysteresis loops at different temperatures were also examined in order to investigate the change of the critical current densities through the magnetic field and temperature increase at 5 and 50K with Bean's model's assistance.

3. Computing and programming

3.1 Lattice parameters calculations

UnitCell software has been used to refine lattice parameters and unit cell volume from powder diffraction data. It utilizes a nonlinear least squares method, which allows carrying out the refinement on the observed X-ray powder diffraction data, presenting a method which minimizes residuals in the experimentally determined quantity (usually $2\theta_{hkl}$). This software gives information about the propagation of the error resulting from the calibration procedure that considered in the estimation of the total uncertainty of the lattice parameters of the actual sample under investigation. The standard deviations (σ) and the U95% uncertainties of measurement at the 95% confidence level are calculated from UnitCell software as mentioned in [47, 48].

3.2 Winfit program

Rietveld refinement of the obtained XRD patterns was performed using Winfit software, to make a deconvolution of the samples diffractograms. Additionally, it was utilized for crystallites size and strain calculations using a single line (max. peak) in the XRD pattern according to the relation ($\varepsilon=\frac{\beta}{4\ tan\theta}$), ε: strain and β: the peak broadening [48].

4. Results and Discussions:

4.1. X-ray characterization:

The normalized [x= $\frac{a-a_{min}}{a_{max}-a_{min}}$], (x is the normalized value of the intensity, a is the intensity value, a_{min} is the minimum value obtained in the intensity, a_{max} is the maximum value obtained in the intensity)[49] X-ray diffractograms of BSCCO system with different concentrations from Bi_2Te_3 nanoparticles $(Bi_{1.6}Pb_{0.4}Sr_2Ca_2Cu_3O_{10+\delta})_{1-x}/(Bi_2Te_3)_x$, (x = 0.0,0.01, 0.02, 0.03) named as (2223, $2223/(Bi_2Te_3)_{0.01}$, $2223/(Bi_2Te_3)_{0.02}$and $2223/(Bi_2Te_3)_{0.03}$) are shown in Figure (1). The identified phase was the Bi-2223 and Bi-2213 of orthorhombic system according to the JCPDS card No. 42-0514 for (BiPb-2223) and JCPDS card No.45-1224 for (Bi-2213) respectively, as depicted in Figure (1). Maqsood et al. show in their work (card No. 42-0514), that the doped Bi-2223 with different concentrations of Pb composed from many mixed phases at different T_c temperatures [50]. One of these phases was the low T_c phase Bi-2212 due to its stability and the other one was the higher T_c phase Bi-2223 [50].On the other hand, Ran et al., in the card No.45-1224 for (Bi-2213), explained that (Bi-2213) consists of two phases (Bi-2223&Bi-2212) in the ratio 1:2 with onset diamagnetic transition at T_c=80K [51]. Besides, unidentified minority phases of non-superconducting compound are not investigated for these systems. It is appeared that there is not any signs/peaks belongs Bi_2Te_3 which confirm that the nanocrystal of Bi_2Te_3 solute into the BSCCO matrix successfully. Even though $Bi_2Sr_2Ca_2Cu_3O_{10+\delta}$ HTSC material classified as one of most significant superconductors employed in a lot of practical applications but it still has a lot of limitations, especially single phase-production, owing to:

(i) The Bi-2212 ($Bi_2Sr_2CaCu_2O_{8+\delta}$) has more thermodynamic stability at the temperature range of preparation than that of (Bi-2223); thus, it typically has the majority phase [50, 51, 52] as well as the peaks overlapping between BSCCO phases exhibit the difficulty in volume fractions calculations.

(ii) The stabilization temperature range of the Bi-2223 phase is very sensitive and limited in several synthesis techniques [53]. So Pb was utilized in doping the stoichiometric Bi-2223 samples before Bi_2Te_3 additive to hopefully make them more stable and enhance high T_c phase volume fraction. It is appeared that Bi-2223 was appeared in the prepared samples as compared with JCPDS cards. But Bi-2212 ($Bi_2Sr_2CaCu_2O_{8+\delta}$) phase was also confirmed to be existed too as the highest ratio in Bi-2213 phase.

(iii) The Oxygen deficiency possibly will create secondary phases in the obtained compositions due to the modulated displacement in Bi_2O_2 and calcium layers

consistent with Oxygen atoms of CuO_2 planes, where the presence of defects can substantially change the charge distribution in the CuO_2 planes [54]

It seems that the addition of Bi_2Te_3 concentration can affect the rate of reaction, which restricts slightly the formation of Bi-2223. This fact suggests that the Bi_2Te_3 nanoparticles addition leads to a change in the homogeneity of the transient liquid forming, its viscosity and the reaction rate of the Bi-2223 phase. According to the XRD spectra, peaks assigned to the Bi_2Te_3 phase admixture was not detected even with high Bi_2Te_3 nanoparticles amounts. Moreover, after the calculated of the lattice parameters and unit cell volumes are obtained, as listed in Table (1). As shown in Table (1), a considerable change was detected in the unit cell volume calculations and c lattice parameters for both BSCCO phases, which prove the effectiveness of the additive of nano- Bi_2Te_3 fit into the structure of Bi-2223. Due to the difficulty of the phase separation of HTSC BSCCO phases, their volume fractions are approximated equal in values even though Bi_2Te_3 nanoparticles concentrations increase (Table (1)).

These results indicate that the small amounts of nano- Bi_2Te_3 additive participate effectively in the phase stability of the BSCCO systems and may slightly affect the low T_c phase (Bi-2212) to the high T_c phase (Bi-2223) ratios. We claim that the effect of Bi_2Te_3 nanoparticles in this situation on the Bi-2223 phase may support in stabilizing the Bi-2223 phase formation due to the existence of Bi which looks like Pb doping. The existence of several inequivalent Cu positions in Bi-2223 unit cell (in the inner and outer planes) plus the understanding of Bi and Te's solubility's on the different sites; consequently, it is believed that Bi of Bi_2Te_3 may occupy Bi site in BSCCO unit cell. Also, it is known that the structural properties and grain connectivity of the Bi-2223 systems are weakened by adding Bi nanoparticles [55]. It is claimed that Te behaves like the transition metals, which may prefer to occupy the outer Cu sites; otherwise, it is also expected that Te could prefer to be positioned adjacent to the outer planes containing oxygen [56]. Furthermore, the c lattice parameter was slightly varied. It was detected due to nano- Bi_2Te_3 addition, which makes a significant change in the hole concentrations in the CuO_2 planes, which has no strong effects on the transition temperatures of BSCCO phases.

The lattice strains were also affected due to the additions of Bi_2Te_3 nanoparticles, which are observed in Figure (2), which shows the maximum peak shifts. The addition

of Bi_2Te_3 nanoparticle causes XRD peaks to shift to lower angle. This result may be related to the changes of the peak broadening and the grain size of the samples. The maximum peak shift, the lower intensity, the max increase in the FWHM of the main peak indicating the lower grain size, and the maximum unit cell volumes was obtained for 2 %wt sample that confirm the data estimated from Winfit program (Table (1)). This may imply the strong interactions between Bi_2Te_3 nanoparticles and BSCCO matrix and the impact on the bond lengths and increasing in the interplane coupling.

Besides, Table (1) illustrates the highest value for the strain for (Bi_2Te_3 with x=0.03). This comprises that optimizing the appropriate quantity of Te doping into Cu sites does not strongly impede the pathways of the reactions for Bi-2223 formation phase. Additional information and investigations were figured out from the given results acquired from the magnetization measurements and is reported below.

3.2 Scanning Electron Microscopy (SEM)

SEM micrographs of the samples are presented in Figures (3a& b) and (3d& e). The analysis of fracture micrographics in these samples also indicates changes in both the grain size and the grain orientation. Also, This SEM analysis observes the non-uniform phase on its surface. But some areas show layer structure estimated belonging to crystal structure of BPSCCO system. Sample also forms a porous material.

In the obtained samples, a plate-like nature of grains, typical of HTSC Bi-based superconductors is observed. The lamellar structure, characteristic of high critical temperature superconductors, is also visible in many grains, while with the Bi_2Te_3 addition the grain size slightly decreases and porosity increases. The average size of the grain is estimated, from image j software, ranging from micro to nanoscale (40: 90 nm) that confirms the obtained data from XRD. The morphology of the grains slightly changes with Bi_2Te_3 content (1–3 %). It is to be noticed that the 1 % added sample shows a microstructure and nanostructures with randomly distributions with highly dense packed grains aligned and are much larger. The sample with x=0.03 provides aggregations between the small grains with different sizes that distributed randomly on the surface of the sample. The black regions are randomly distributed in the matrix structure, which indicates a weaker link between the grains.

The addition of Bi_2Te_3 nanoparticles may impact the surface morphology and the average size of BSCCO. This is what was expected; the Bi_2Te_3 compound at these low concentrations seems to find its way into the grain boundaries and introduce new

artificial boundaries decreasing slightly the average size of the BSCCO crystallites. The grains are distributed randomly or we can say that the grains in the specimen are oriented anisotropically and poorly connected. On the other hand, Figure (3c &f) presents the EDX spectrum of the surface of the samples with 1 % and 3 % of Bi_2Te_3 addition, which shows that the main elements of the grains are Bi, Pb, Sr, Ca, Cu, Te, and O, atoms. These results indicate the incorporation of Bi and Te into the BSCCO lattice and reveal that the elemental composition of all the samples does not contain any foreign element. It is seen that from EDX data that the ratio of Bi and Te increases slightly with the increase of Bi_2Te_3 nanoparticles. It supposed that Bi_2Te_3 to melt and diffuse inside sample since its melting temperature (T_m = 585°C) lower than the sintering temperature.

3.3 Transmission Electron Microscopy (TEM) images

Figures (4a-c) portray the TEM images of $(Bi_{1.6}Pb_{0.4}Sr_2Ca_2Cu_{3-y}O_{10+\delta})_{0.99}/(Bi_2Te_3)_{0.01}$ sample, which exhibits the formation of BSCCO thin micro-sheet with tiny particles in the background in different sizes ranging from nano to microns (Figure 4c) . It is clear from SEM & TEM images for the inter-planar distances were ranging from a few nm, which were assigned to the lattice planes for the orthorhombic crystal structure, which confirmed XRD data. HTSC materials, especially BSCCO phases has double or triple CuO_2 planes, have remarkable microstructural and morphological characteristics due to its incommensurate modulation structure (which is common for these perovskite materials [57:59]). On the other hand, the obtained Figure (4c) shows that Bi_2Te_3 nanoparticles were embedded into the grains of BSCCO polycrystalline materials or more practically between its planes.

These images portrayed the grains of BSCCO with a clear presence of high density tiny accumulated particles from Bi_2Te_3 nanoparticles, as seen in Figure (3c&b). It is suggested that the orientations of these nano-sized particles of Bi_2Te_3 produce significant effects on the superconducting transitions temperatures of the HTCS and also the critical current density (J_c) values compared with an isotropic distribution [60]. It is believed that the self distributions of the nanoparticles into the BSCCO planes during the composite processing make them promising to be used in applications. The obtained results confirmed the data obtained from SEM and XRD.

3.3 Magnetization measurements

Temperature dependence magnetic response for Zero field cooled (ZFC) / field cooled (FC) of the present samples between 4 K and 120 K are shown in Figure (5). Figure (5) reveals M-T and dM/dT versus T measurements for $(Bi_{1.6}Pb_{0.4}Sr_2Ca_2Cu_{3-y}O_{10+\delta})_{1-x}/(Bi_2Te_3)_x$ with (x=0.00,0.01,0.02,0.03) systems, which proves so well the superconducting diamagnetic signal for double transitions from high-T_c phase Bi-2223 and the low-T_c phase (Bi-2212). T_{c1} and T_{c2} for each phase were observed from (M-T) measurements Table (1). These results reveal that the existence of the two BSCCO phases as discussed before in XRD where Bi-2213 phase composed of high and low T_c phases, as mentioned in ref. [45]. In both cases for (ZFC/FC) in Figure (5), the diamagnetic signal decreases with the addition of Bi_2Te_3 nanoparticles, and reaches a minimum value for 1% wt. of Bi_2Te_3 additive. The achieved results for the shift in diamagnetic signals may be associated with the weak coupled between the grains in 2223 samples [61].

The highest signal was remarked for 3 %wt. Bi_2Te_3 amongst the doped samples. Also, it is claimed that Bi_2Te_3 additive may also influence the characteristics of the BSCCO phases negatively. But on the other hand, it enhances the transition temperature and the phase stability of the lower phase Bi-2212 (T_{c2}) (Table (1)). T_{c1} and T_{c2} depend on the local structure and are robustly influenced by the charge densities redistribution through the CuO_2 planes, including their adjacent layers, which are regarded as a charge reservoir. The eliminations of Oxygen form Cu-O chains create an imbalance in the charge distributions through the planes, so it is expected that the slight changes in T_c and the lattice parameters as well.

The minor obtained changes in the onset transition temperatures were investigated and proposed within the experimental error where the diamagnetic signal for the low T_c- phase was sharper than the higher T_c- phase. This give us different interpretations for the volume fractions of BSCCO phases observed in XRD analysis which does not reflect the ratios of the phases of BSCCO in magnetic properties. Many reasons could help in understanding this effect: i) This could be due to the insufficient duration of sintering time to optimize the formation of high T_C phase [62], ii) This decreasing of T_c attributed to the decrease of hole concentration in the Cu-O plane caused by the Bi_2Te_3 nanoparticles dopant which providing additional electrons that in turn decrease the hole carrier concentration due to the interaction of Te^{2-} ions with BSCCO matrix that leading to affect on diamagnetic signal and other superconducting

properties [63], iii) This may imply to the characterization the superconducting thermodynamic fluctuations [64] or the opening of spin-gap that appears in the HTSCs due to magnetic impurity substitutions [65]. These superconducting thermodynamic fluctuations occur at finite temperatures just above T_c due to the appearance of Cooper pairs even above this temperature [66]. The highest achieved magnetization signal was registered for the pure sample and the 1 % wt Bi_2Te_3 sample, which may be attributed to the solubility limit of Bi_2Te_3 into the BSCCO matrix [56].

The (M–H) hysteresis cycles for the undoped/doped BSCCO pellets with Bi_2Te_3 nanoparticles are obtained at two distinctive temperatures, 5 and 50 K, in a magnetic field of ±15 KOe (Figure (6)). The obtained samples were cooled at zero field, and then the external magnetic field was oriented perpendicular to the plane of the samples swept up to H_{ext} = 15 KOe, then to H_{ext} = -15 kOe and back to H_{ext} = 15 kOe again. The determined magnetization confirms the performance typical for a high-temperature superconductor with strong pinning. Typically, the magnetization (M) at a fixed external field obviously associated with the field sweep direction. This indicates that the external field's magnitude and direction play a significant role in the current density changes.

The hysteresis loops of the obtained samples demonstrate wider loops at 5 K than that obtained at 50 K that may indicate the doping effect of Bi_2Te_3 nanoparticles in the matrix of BSCCO. Also, the pure sample shows the widest one in both hysteresis loops at 5 and 50 K, respectively.

Generally, Figure (6) exhibits a small symmetrically an incensement around -5000 Oe and +5000 Oe which assigned to a magnetic field-induced enhancement of the irreversible magnetization called ‘‘second magnetization peak’’ SP which common in HTSC. The investigation of this effect of controlled disorder on both the SP observed in the irreversible magnetization at temperatures below 35 K and the closely related jump in the reversible magnetization identifying the first order transition in the highly anisotropic BSCCO. BSCCO has lead to the general acceptance of a phenomenological phase diagram of the vortex lattice containing three distinct phases: the vortex liquid, the crystalline and glassy solid phases which related to [67, 68] the phases transition from a quasi-ordered low magnetic field phase to a disordered high field phase [67, 69].Through the swept field, the critical state was established (full flux penetration throughout the sample). The lower branch of the loop was subsequently measured as the

field was ramped from 0 Oe to ±10 kOe, and the upper branch was collected as the field was swept back down. The curves of the samples with/without Bi_2Te_3 additions exhibit a distinct shape with a conspicuous feature: a second magnetization peak (SP) at ±5 kOe. In general, this shape and the magnitude of the magnetization is indicative of a vortex pinning regime at low fields below ±5 kOe and get stronger pinning at higher fields. The source of pinning is likely point defects in the Bi-O layer—specifically, oxygen interstitials and Bi vacancies [67: 69] , and this should be the main source of disorder in the bulk that hinders thermal wandering of vortices.

In HTSC crystals, a surface barrier—called the Bean-Livingston (BL) barrier—often plays a significant role in determining the magnetic properties and shaping the M(H) loops [70,71]. It originates from competing effects: vortices are repelled from the surface by Meissner shielding currents and attracted by a force arising from the boundary conditions (usually modeled as the attraction between the vortex and an image antivortex [72]). On the other hand, wider hysteresis loops in the critical state picture can entail both larger J_c's and/or larger grain size. Furthermore, the strong flux pinning and more well-defined anisotropy.

The inductive critical current density J_c (A/m^2) or the magnetic critical current J_c have been computed from DC magnetization of hysteresis loops of a fixed temperature and slow field sweep. The expression linking the hysteresis loop opening ΔM and J_c includes assumptions on $J_c(H)$ dependencies collectively according to the critical state models. Also, the geometry of sample appears into the formula. J_c values for the investigated samples were calculated using the following formula [73]:-

$$J_c = \frac{20\,\Delta M}{a(1-a/3b)} \qquad (1)$$

J_c signifies the critical current density in A/m^2, ΔM represents the width of the magnetization hysteresis loop in emu/cm^3 and a, b symbolize the side dimensions of pellet in cm. This expression is used to evaluate the critical current density for the isotropic superconducting materials with rectangular shape cross-sections positioned in the plane perpendicular to the external magnetic field [73]. Figure (6) concludes that the ΔM for the hysteresis loops decrease with increasing the temperatures, which characterize the critical current density due to Bean's model by assuming an identical and steady current density throughout the entire sample.

Improvement of M-H performance in HTSC considerably relies on creating the well crystallizations of superconductors' grains, including the inter-granular conductivity, and the volume fraction of the preferred phases. In order to enhance the magnetization hysteresis loops at high temperatures, they are generally related to the achievement of the flux pinning properties in intra-grain regions, involving M-H curves with larger areas [74, 75]. The standard diamagnetic signal of type II superconductors is obviously obtained in all the samples, revealing that the desired superconducting phases are achieved. Both the pure sample and the sample with 3 % wt. of Bi_2Te_3 concentration display a large M-H, in comparison with the other samples, indicating the enhancement of better electrical connectivity between the grains of superconducting material, the existence of high amounts of superconducting phases, and the formation of the pinning centers effectively in the perfect amounts. On the contrary, 1% wt. with Bi_2Te_3 content illustrates a smaller diamagnetic performance in M-H loops, indicating weak grain connections and a low degree of crystallinity.

It is well-known that the hysteresis loops in the low-field region is related to the inter-grain currents, whereas that for the high-field region is correlated to the intra-grain currents. The irreversible magnetic moments include contributions of both inter- and intra-granular [76]. Because the obtained samples show the polycrystalline nature, and the inter-grain connectivity verifies the bulk critical current density (J_c) to a large extent. Figure (7) illustrates the critical current density values calculated from the magnetization hysteresis loops results. J_c of 2223 and Bi_2Te_3-addittive samples decrease drastically with the increase of the magnetic fields because of the demolition of weak links in higher magnetic fields between the grains and the pinning effect, which related to the misorientation of the grains and improve of the local structural distortions, including the lattice strains and porosity as well [77]. For both 5 &50 K results, the pure sample 2223 has the highest critical currents density (1.5×10^4 and 350 A/cm^2, respectively), where the sample with (1% wt. Bi_2Te_3) has the lowest critical current density values (4×10^3 A/cm^2) at 5 K. On the other hand, for 50 K, sample with (2% & 3%wt Bi_2Te_3) registered the lower values of J_c (98 & 100 A/cm^2, respectively). The values of J_c of the higher concentrations of Bi_2Te_3 overlapped at the higher values of J_c for 50 K. Phase analysis and identifications by XRD obviously confirms that there are no impurity phases from Bi_2Te_3 nanoparticles. Therefore, the nano-sized Bi_2Te_3 as a secondary phase can colonize in intra-grains and among the inter-grain regions as seen and confirmed from

TEM images, producing poor crystallinity rather than the creation of new efficient pinning centers in the samples.

Although Bi_2Te_3 nanoparticles don't have the magnetic nature of the magnetic nanoparticles, it affects on the superconducting parameters and the behavior of BSCCO and the variation of its phase volume fractions. One is supposed to construct a better consideration in understanding the interaction and the solubility of nanoparticles inside the superconductors besides the current-carrying mechanisms in different temperature ranges. Consequently, it is supposed that Bi_2Te_3 nanoparticles may destroy superconductivity and deteriorate their current carrying capability when diffuse into the BSCCO system which is seen in Figures (6 & 7) and lowering the J_c like the behavior of the magnetic nanoparticles [78].

Representative plots achieved for pure sample 2223 and 2223 with various concentrations from Bi_2Te_3 samples at 5 &50 K are depicted in Figure (8). An avalanche of flux is observed in the (M–H) hysteresis loops, resulting from the increasing and decreasing magnetic field. This flux avalanche behavior has been articulated earlier in BSCCO when local adiabatic conditions and the additive of various kinds from nanoparticles are satisfied [42, 44, 45, 79]. The pure BSCCO which have the lower vortex pinning centers have the higher values for both measured temperatures (5 &50 K). The Bi_2Te_3 nanoparticles have remarkable impact on both the connectivity and BSCCO matrix structure, so the effective sign of it appears clearly on the J_c as well as $Jc^{0.5} H^{0.25}$ determinations as seen in Figure (8).

In general, $H_{irr}(T)$ is defined as a crossover field that separates the solid vortex region from the liquid vortex region. In other words, $H_{irr}(T)$ is donated as the field above which vortex depinning starts. At the same time, $H_{c2}(T)$ is the crossover field between the superconducting and the normal state of the superconducting materials. But in the low-temperature superconductors, these two fields are almost the same and consequently, H_{c2} (T) is typically used as a scaling field. Conversely, for intermediate and high-temperature superconductors, this liquid vortex region appears, and hence, pinning force cannot be characterized above the depinning line (viz., above H_{irr} (T)). Thus, in this class of superconductors, irreversible field (H_{irr} (T)) is commonly exploited as the scaling field in place of $H_{c2}(T)$ [80]. In order to investigate J_c–H behavior of

Bi_2Te_3 added 2223, the irreversible field (H_{irr}) for the obtained set of samples are estimated by the assistance of Kramer plot (viz., $J_c{}^{0.5}H^{0.25}$ vs. H) at T=5 &50 K. H_{irr} is determined by extrapolating the linear portion of the Kramer plot up to the field for which $J_c^{0.5}$ $H^{0.25}$ reaches to zero [81, 82]. Figure (8) illustrates plots of schematic representations for the obtained set of samples at 5 & 50 K, where Figure (9) shows the calculated irreversible fields H_{irr} with different Bi_2Te_3 weight percents. The highest value of H_{irr} was for the pure sample 2223 and there were a slightly deviations in the values of the Bi_2Te_3 additive samples as seen into Figure (9).

In order to acquire further information about the effective pinning mechanism, the J_c results make it possible to gain additional insight into the origin of improved pinning characteristics and estimate the pinning force density (F_p) by $F_p=J_c\times\mu_0H$ [79, 80]. Figure (10) illustrates the pinning force density for all samples at 5 K. Particularly, the flux pinning strength affects strongly due to the existence of the number of pinning centers, the changes in structure and size. As remarked into Figure (10), the maximum field (H_{max}) and the maximum force ($F_{P\text{-}max}$) was determined for each sample. Bi_2Te_3 with x= 0.01 has the lower $F_{P\text{-}max}$ and compared to other ones while H_{max} was nearly the same for all samples, as depicted in Figure (10). The H_{max} relates to the magnetic field at which the F_P reaches its maximum. It is known that the higher H_{max} specifies the stronger pinning strength and the best performance in the 2223 sample is partly produced by the improvement of H_{max}.

Here, H_{max} and $F_{P\text{-}max}$ reduce with Bi_2Te_3 concentration increase, implying a reduction in flux pinning with the additive of Bi_2Te_3 nanoparticles. It is significant to mention that the flux pinning strength can be controlled by verifying the additive materials as pinning centers and their proper concentration. The obtained result of this study denotes a high efficiency of flux pinning by Bi_2Te_3 nanoparticles.

To find out the pinning mechanisms, the normalized magnetic field ($h=H/H_{max}$) dependence of flux pinning strength ($f_p=F_P/F_{P\text{-}max}$) was investigated. Owing to Dew Huges [84], flux pinning force in type II superconductors is generally manipulated by the superconducting nature and also the size of the pinning centers, including the microstructure parameters and the flux lattice rigidity. Also, this model basically discussed the two types that affect on the pinning centers [85]: (i) the non-superconducting phases or the normal particles which embedded/added into the

superconducting matrix influencing on the scattering of the electron mean free path. (ii) The shift in the superconducting transition temperature (T_c). Eqs. (2)–(4) represents three theoretical models which are often used to analyze the experimental data of f_p-h of the obtained samples [83,85,86]:

$$f(h) = \frac{9h}{4}(1 - \frac{h}{3})^2 \quad \text{normal point pinning} \quad (2)$$

$$f(h) = \frac{25\sqrt{h}}{16}\left(1 - \frac{h}{5}\right)^2 \quad \text{surface pinning} \quad (3)$$

$$f(h) = 3h^2(1 - \frac{2h}{3}) \quad \Delta k \text{ pinning} \quad (4)$$

Figure (11) illustrates f_p vs. h curves for all the samples with different Bi_2Te_3 wt. % at 5 K. The curves for the experimental and theoretical data were estimated by Eqs. (2)–(4) are depicted in the Figure to figure out the flux strength. For the fields less than and beyond h_{max}, the data points for the pure and lower Bi_2Te_3 concentrations samples scale positioned between the normal point pinning and Δκ pinning where the highest ratio 3 % wt Bi_2Te_3 sample placed between surface pinning and normal point pinning at lower fields and higher than all pinning beyond h_{max}. The data between point and $\Delta\kappa$ pinning are scattered, which concluded that the presence of Δκ pinning is not accurately exist due to the limitation in the obtained data higher than h_{max}. In contrast, the similarity between the theoretical and the experimental date of f_p plots in the samples with and without Bi_2Te_3 nanoparticles implies the activation of surface and point mechanisms because of the crossing between Bi_2Te_3 nanoparticles and the vortices. The surface grains of the superconductors are well-aligned at the low field and can be regarded as pinning centers. The superconductors' surface grains are well-aligned at the low field and can regard as pinning centers. This consequence shows the role of Bi_2Te_3 additive in strengthening pinning centers' contribution in flux pinning characteristics and the substantial enhancement in J_c.

4- Conclusion

The achieved results have raised two interesting propositions for Bi_2Te_3 nanoparticles interaction with the granular BSCCO superconducting network. Firstly, the volume fraction of the Bi-2223 phase and Bi-2212 phase changes to each other slightly with the increases of Bi_2Te_3 nanoparticles. Bi_2Te_3 nanoparticles added samples showed a significant impact on the lattice parameters and the other microstructures parameters compared with a non-added sample. Although the onset temperatures of BSCCO phases were not affected strongly due to the existence of Bi_2Te_3 nanoparticles,

the lower diamagnetic transition was registered for (Bi_2Te_3 with x=0.01).Secondly, According to the magnetic measurements, the pure sample shows the highest J_c values (1.5 $X10^4$ and 350 A/cm^2 at 5 and 50 K, respectively), H_{irr} , H_{max} and $F_{p\text{-}max}$ compared to the other samples. These results prove the impact of Bi_2Te_3 nanoparticles on the magnetic and superconductors characteristics. Although the non-magnetic nature of Bi_2Te_3, it is believed that Bi_2Te_3 nanoparticles affected on the flux pinning, the hysteresis loops widths and the critical currents densities. This finding is very motivating because the depinning line in the BSCCO system lies much below T_c, even in zero magnetic fields.

References:

[1] M.K. Wu, J.R. Ashburn, C.J. Torng, P.H.Hor, R.L.Meng, L.Gao, Z.J.Huang, Y.Q. Wang and C.W.Chu, Superconductivity at 93 K in a new mixed-phase Y-Ba-Cu-O compound system at ambient pressure, Phys. Rev. B. 58 (1987) 908-910. https://doi.org/ 10.1103/ PhysRevLett.58.908.

[2] H. Maeda,V.Tanaka,M.Fukutomi and T.Asano, A new high-r. oxide superconductor without a rare earth element, Jpn.J.Appl.Phys. 27 (1988) L209-210.

[3] T. Masuda, T. Kato, H. Yumura, M. Watanabe, Y. Ashibe, K. Ohkura, C. Suzawa, M. Hirose, S. Isojima, K. Matsuo, S. Honjo, T. Mimura, T. Kuramochi, Y. Takahashi, H. Suzuki, T. Okamoto, Verification tests of a 66 kV HTSC cable system for practical use (first cooling tests, Physica C. 378–381 (2002) 1174-1180. https://doi.org/10.1016/S0921-4534(02)01750-1.

[4] O. Tonnesen, M. Daumling, K.H. Jensen, S. Kvorning, S.K. Olsen, C. Traholt, E. Veje, D. Willen, J. Ostergaard, Operation experiences with a 30 kV/100 MVA high temperature superconducting cable system, Supercond. Sci. Technol. 17 (2004) S101. https://doi.org/10.1088/0953-2048/17/5/002.

[5] Y. Xin, B. Hou, Y.F. Bi, K.N. Cao, Y. Zhang, S.T. Wu, H.K. Ding, G.L. Wang, Q. Liu, Z.H. Han, China's 30 m, 35 kV/2 kA ac HTS power cable project, Supercond. Sci. Technol. 17 (2004) S332. https://doi.org/10.1088/0953-2048/17/5/048.

[6] T. Kurusu, M. Ono, S. Hanai, M. Kyoto, H. Takigami, H. Takano, K. Watanabe, S. Awaji, K. Koyama, G. Nishijima, K. Togano, A cryocooler-cooled 19 T superconducting magnet with 52 mm room temperature bore, IEEE Trans. Appl. Supercond. 14 (2004) 393. 10.1109/TASC.2004.829679.

[7] M.C. Cheng, B.P. Yan, K.H. Lee, Q.Y. Ma, E.S. Yang, A high temperature superconductor tape RF receiver coil for a low field magnetic resonance imaging

system, Supercond. Sci. Technol. 18 (2005) 1100. https://doi.org/10.1088/0953-2048/18/8/013.

[8] K. Suzuki1, J. Baba, T. Nitta, Conceptual design of an SFCL by use of BSCCO wire J. Phys. Conf. Ser. 97 (2008) 012293. https://doi.org/10.1088/1742-6596/97/1/012293.

[9] B.A. Albiss, Thick films of superconducting YBCO as magnetic sensors, Supercond. Sci. Technol. 18 (2005) 1222. https://doi.org/10.1088/0953-2048/18/9/014.

[10] B.A. Albiss, M. Gharaibeh, I.M. Obaidat, N. Al-Rawashdeh, R. Oweis, N. Hamdi, M.K. Hasan (Qaseer), Magnetotransport and structural properties of superconducting BPSCCO thick film on MgO substrate, Phys. Status Solidi a. 205 (2008) 1851.

[11] C. Terzioglu, M. Yilmazlar, O. Ozturk, E. Yanmaz, Structural and physical properties of Sm-doped $Bi_{1.6}Pb_{0.4}Sr_2Ca_{2-x}Sm_xCu_3O_y$ superconductors, Physica C. 423 (2005) 119–126.

[12]R.P. Aloysius, P. Guruswamy and U. Syamaprasad, Enhanced critical current density in (Bi,Pb)-2223 superconductor by Nd addition in low percentages, Physica C. 426–431(2005) 556–562.

[13]H. Sozeri, N.Ghazanfari, H. Ozkan, A. Kilic, Enhancement in the high-T_c phase of BSCCO superconductors by Nb addition, Supercond. Sci. Technol. 20 (2007) 522–528.

[14]. S.A. Halim, S.B. Mohamed, H. Azhan, S.A. Khawaldeh, H.A.A. Sidek, Effect of barium doping in Bi–Pb–Sr–Ca–Cu–O ceramics superconductors, Physica C. 312 (1999) 78–84.

[15]J. W. Ekin, A. I. Braginski, A. A. J. Panson, M. A. Janocko, D. W. CaponeII, N. J. Zaluzec, B. Flandermeyer, O. F. de Lima, M. Hong, J. Kwo, S.H.Liou, Evidence for weak link and anisotropy limitations on the transport critical current in bulk polycrystalline $Y_1Ba_2Cu_3O_x$, J. Appl. Phys. 62 (1987) 4821. https://doi.org/10.1063/1.338985.

[16]P. Chadhari, J. Mannhart, D. Dimos, C. C. Tsuei, J. Chi, M. M. Oprysko, M. Scheuemann, Direct measurement of the superconducting properties of single grain boundaries in $Y_1Ba_2Cu_3O_{7-\delta}$, Phys. Rev. lett. 60 (1988) 1653. https://doi. org/10. 1103 / PhysRevLett.60.1653

[17] D. Darminto, M. O. Tjia T. Motohashi, H. Kobayashi, Y. Nakayama, J.Shimoyama, K. Kishio, Effects of Pb substitution on the vortex state of oxygen-overdoped $Bi_2Sr_2CaCu_2O_{8+\delta}$ single crystal Phys. Rev. B 62 (2000) 6649–6655. 10.1103/PhysRevB.62.6649.

[18] G. D. Guy, Z. W. Liny, G. J. Russelly, N. Koshizukaz, Effect of Fe on the crystal growth morphology of Bi-Sr-Ca-Cu-O,Supercond. Sci. Technol. 11, (1998) 1129-1132. https://doi.org/10.1088/0953-2048/11/10/051.

[19] X. H. Chen, S. Y. Li, K. Q. Ruan, Z. Sun, Q. Cao, and L. Z. Cao, Effect of doping on the anisotropic resistivity in single-crystal $Bi_2Sr_2CaCu_2O_{8+\delta}$ with Fe, Co, and Ni,Phys. Rev. B. 60 (1999) 15339–44. https://doi.org/10.1103/PhysRevB.60.15339

[20] H. Maeda, W. P. Chen, T. Inaba, M. Sato, K. Watanabe and M. Motokawa, Texture development in Bi-based superconductors grown in high magnetic fields and its effect on transformation of Bi(Pb)2212 to Bi(Pb)2223,Physica C: Superconductivity. 354 (2001) 338-341. https://doi.org/10.1016/S0921-4534(01)00050-8.

[21] S. K. Sinha, S. C. Gadkari, S. C. Sabharwal, L. C. Gupta and M. K, Gupta, Bulk synthesis of $(BiPb)_2Sr_2Ca_2Cu_3O_x$ superconductor Physica C: Superconductivity. 185-189 (1991) P 499-500. https://doi.org/10.1016/0921-4534(91)92052-D

[22]J. Shimoyama, Y. Nakayama, K. Kitazawa, K. Kishio, Z.Hiroi, I. Chong and M.Takano, Strong flux pinning up to liquid nitrogen temperature discovered in heavily Pb-doped and oxygen controlled Bi2212 single crystals,Physica C. 281(1997) 69-75. https://doi.org/10.1016/S0921-4534(97)00471-1.

[23] A. V. Narlikar, Studies of high temperature superconductors, 1-10, New York: NOVA Science Publishers, 1997.

[24] J. M. Tarascon, B. G. Bagley, in chemistry of superconductor Materials, edited by T. A. Vanderah (New York: NOYES Publishers), 1993, P-310.

[25]A. G. Mamalis, S. G. Ovchinnikov, M. I.Petrov, D. A. Balaev, K A Shaihutdinov, D. M. Gohfeld, S. A.Kharlamova and I. N.Vottea, Composite materials on high-T_c superconductors and $BaPbO_3$, Ag basis, Physica C. 364 (2001) 174-7. https://doi.org/10.1016/S0921-4534(01)00749-3.

[26] I. Chong, Z. Hiroi, M. Izumi, J. Shimoyama, Y. Nakayama, K. Kishio, T. Terashima, Y. Bando and M. Takano, High Critical-Current Density in the Heavily Pb-Doped $Bi_2Sr_2CaCu_2O_{8+\delta}$ Superconductor: Generation of Efficient Pinning Centers, Science. 276 (1997) 770-773. https://doi.org/10.1126/science.276.5313.770.

[27] P. M. Sarun, S. Vinu, R. Shabna, A. Biju, P. Guruswamy, U. Syamaprasad, Influence of Ho-Doping on the Electromagnetic Field-Dependent E–J Characteristics of (Bi,Pb)-2212 Superconductor,IEEE Transactions on Applied Superconductivity, 19 (2009) 35-38. doi: 10.1109/TASC.2008.2010866.

[28] X. Y. Cai, A. Gurevich, D. C. Larbalestier, R. J. Kelley, M. Onellion, H. Berger, and G. Margaritondo, Static and dynamic mechanisms of the anomalous field dependence of magnetization in Bi-Sr-Ca-Cu-O and Bi-Pb-Sr-Ca-Cu-O single crystals, Phys. Rev. B. 50 (1994) 16774-16777. https://doi.org/10.1103/PhysRevB.50.16774.

[29] M.H. Pu, W. H Song, B. Zhao, X. C. Wu1, T. Hu, Y P Sun1 and J.J.Du, Enhanced flux pinning in (Bi, Pb)-2223/Ag tapes by slight Pr substitution, Supercond. Sci. Technol. 14 (2001) 305-310.

[30] Z.Y. Jia, H.Z. Tang, Q.Y. Yang, T. Xing, Y.Z. Wang, G.W. Qiao, Effects of nano-ZrO_2 particles on the superconductivity of Pb-doped BSCCO, Physica C. 337, (2000)130. https://doi.org/10.1016/S0921-4534(00)00072-1.

[31] A. Ghattas, M. Annabi, M. Zouaoui, F. Ben Azzouz, M. Ben Salem, Flux pinning by Al-based nano particles embedded in polycrystalline (Bi,Pb)-2223 superconductors Physica C. 31(2008) 468. https://doi.org/10.1016/j.physc.2007.10.006.

[32] E. Guilmeau, B. Andrzejewski, J.G. Noudem, The effect of MgO addition on the formation and the superconducting properties of the Bi2223 phase, Physica C. 387(2003) 382. https://doi.org/10.1016/S0921-4534(02)02360-2.

[33] A. Ghattas, M. Zouaoui, M. Annabi, A. Madani, F. Ben Azzouz, M. Ben Salem, Enhancement of superconductivity properties in nano ZrO_2 particles added $Bi_{1.8}Pb_{0.4}Sr_2Ca_2Cu_3O_x$ ceramics, J. Phys. Conf. Ser. 97 (2008) 012179. https://doi.org/10.1088/1742-6596/97/1/012179.

[34] H. Baqiah, S.A. Halim, M.I. Adam, S.K. Chen, S.S.H. Ravandi, M.A.M. Faisal, M.M. Kamarulzaman, M. Hanif, The effect of magnetic nanoparticle addition on the superconducting properties of $Bi_{1.6}Pb_{0.4}Sr_2Ca_2Cu_3O_\delta$ superconductors, Solid State Sci. Technol.17 (2009) 81.

[35] A.N. Jannah, H.Abdullah, R. Abd-Shukor, Transport Critical Current Density of $(Bi_{1.6}Pb_{0.4})Sr_2Ca_2Cu_3O_{10}$ Ceramic Superconductor with Different Nanosized Co_3O_4 Addition, Advances in Condensed Matter Physics, vol. 2014, Article ID 498747, 8 pages, 2014. https://doi.org/10.1155/2014/498747.

[36]S. Zhang, X. Ma, B. Shao, L. Cui, G. Liu, H. Zheng, X. Liu, J. Feng, C. Li, P. Zhang, Fabrication of multifilamentary powder in tube superconducting tapes of Bi-2223 with Sr deficient starting composition, Cryogenics 114 (2021) 103245. https://doi.org/10.1016/j.cryogenics.2020.103245.

[37] Y.C. Guo, Y. Tanaka, T. Kuroda, S.X. Dou and Z.Q. Yang, Addition of nanometer SiC in the silver-sheathed Bi2223 superconducting tapes, Physica C. 311(1999) 65-74.

[38] W. Wei, J. Schwartz, K.C. Goretta , U. Balachandran, A. Bhargava, Effects of nanosize MgO additions to bulk $Bi_{2.1}Sr_{1.7}CaCu_2O_x$, Physica C. 298 (1998) 279-288. https://doi.org/10.1016/S0921-4534(97)01889-3

[39] K. Wei, R. Abd-Shukor, Superconducting and Transport Properties of (Bi-Pb)-Sr-Ca-Cu-O with Nano-Cr_2O_3 Additions, Journal of Electronic Materials 36 (2007) 1648–1651. 10.1007/s11664-007-0287-1

[40] M. Annabi, A.M. Chirgui, F. Ben Azzouz, M. Zouaoui, M. Ben Salem, Addition of nanometer Al_2O_3 during the final processing of (Bi,Pb)-2223 superconductors, Physica C. 405 (2004) 25. https://doi.org/10.1016/j.physc.2004.01.012.

[41] H. Sozeri, N. Ghazanfari, H. Ozkan, A. Kilic, Enhancement in the high-T_c phase of BSCCO superconductors by Nb addition, Supercond. Sci. Technol. 20 (2007) 522. https://doi.org/10.1088/0953-2048/20/6/007.

[42] K. Habanjar, F. El Haj Hassan, R. Awad, Physical and dielectric properties of (Bi,Pb)-2223 superconducting samples added with $BaFe_{12}O_{19}$ nanoparticles, Chemical Physics Letters, 757 (2020) 137880. https://doi.org/10.1016/j.cplett.2020.137880.

[43] M.J. Masnita, R. Abd-Shukor, Iron sulfide effects on AC susceptibility and electrical properties of $Bi_{1.6}Pb_{0.4}Sr_2CaCu_2O_8$ superconductor,Results in Physics. 17 (2020) 103177, doi: https://doi.org/10.1016/j.rinp. 2020.103177

[44] D. Brochier, P. Cardinne, M. Renard, Inclusions ferromagnétiques dans des supraconducteurs de deuxième espèce, J. Physique. 29 (1968) 953. 10.1051/jphys:019680029010095300

[45] P.N. Togulev, V.V. Bazarov, I.B. Khaibullin, N.M. Suleimanov, Reinforcement of pinning by surface magnetic microparticles in high-*Tc* superconductors, Low Temp. Phys. 28 (2002) 250.

[46] M.S. Shalaby, N.M. Yousif, H.A. Zayed, H.M. Hashem, L.A. Wahab, The effect of Radiation on Thermal conductivity of Nano-Structured PANI/Bi_2Te_3 Composites, J. Sci. Res. Sci. 36 (2019) 339.

[47] Holland, T., & Redfern, S. (1997). Unit cell refinement from powder diffraction data: The use of regression diagnostics. Mineralogical Magazine, 61(1997) 65-77. doi:10.1180/minmag.1997.061.404.07

[48]M.S.Shalaby, H.M. Hashem, N.M. Yousif, *et al.* Preparation, structural characteristics and optical parameters of the synthesized nano-crystalline sulphur-doped $Bi_2Te_{2.85}Se_{0.15}$ thermoelectric materials. *J Mater Sci: Mater Electron* **31** (2020) 10612–10627 https://doi.org/10.1007/s10854-020-03611-4

[49] C. Kaya, B. Özçelik, B. Özkurt, A. Sotelo, M. A. Madre,Effect of Ce substitution on structural and superconducting properties of Bi-2212 system, J Mater Sci: Mater Electron 24 (2013) 1580–1586 DOI 10.1007/s10854-012-0979-z

[50]A. Maqsood, N.M. Bhatti, S. Ali, I. Haq, Preparation and characterization of Bi-based high T_c superconductors, Mat. Res. Bull., 25 (1990) 779-784. https:// doi.org/ 10.1016/0025-5408(90)90206-H

[51] Z.Y. Ran, C. Chu, On the 110K superconducting phase in the Bi-Sr-Ca-Cu oxide system , Mod. Phys. Lett. B2 (1988) 699. https://doi.org/10.1142/S0217984988000370.

[52] M.S. Shalaby, H.M. Hashem, T.R. Hammad, L.A. Wahab,K.H. Marzouk, S. Soltan, Higher critical current density achieved in Bi-2223 High-Tc superconductors, Journal of Radiation Research and Applied Sciences. 9(2016) 345-351.

[53] P. Majewski, S. Kaesche, F. Aldinger, Fundamentals of the preparation of high-T_C, superconducting $(Bi,Pb)_{2+x}Sr_2Ca_2Cu_3O_{10+\delta}$ ceramics, Adv. Mater. 8 (1996) 764-765. https://doi.org/10.1002/adma.19960080914.

[54]E. Gianini, R. Gladyshevskii, N. Clayton, et al., in Proceedings of the Seventh International Workshop "High-Temperature Superconductors and Novel InorganicMaterials Engineering," Moscow, Russia, *June 20–25, 2004* (Moscow, 2004).

[55] M. Ahangari, V. Daadmehr, Investigation of structural effects of Bi nanoparticle addition on HTSC- BSCCO-2223,Through The sol-gel Method, Journal of Interfaces, Thin Films, and Low dimensional Systems 2 (2017-2018) 51-55. 10.22051/JITF.2018.18628.1016.

[56] A.K. Jha, G. Mendirattra, Mössbaur Study in Bi-Pb-Sr-Ca-Cu-O ceramic superconductor, Solid State Commun. 93 (1995) 79. https://doi.org/10.1016/0038-1098(94)00614-8

[57] S. H. Pan, E. W. Hudson, J. Ma, and J. C. Davis, Imaging and identification of atomic planes of cleaved $Bi_2Sr_2CaCu_2O_{8+\delta}$ by high resolution scanning tunneling microscopy, Appl. Phys. Lett., 73 (1998) 58. https://doi.org/10.1063/1.121722.

[58] M. Lojka, F. Antončík, D. Sedmidubský, T. Hlásek, J. Wild, J. Pavlů, O. Jankovský, V. Bartůněk, Phase-stable segmentation of BSCCO high-temperature superconductor into micro-, meso-, and nano-size fractions, j. mater. res. technol. 9 (2020)12071–12079. https://doi.org/10.1016/j.jmrt.2020.08.107

[59] I. Verma, R. Kumar, V. Ganesan, *et al.*, Synthesis and Magnetic Properties of $(Bi, Pb)_2Sr_2Ca_2Cu_3O_{10+\delta}$ Superconductor, J. Supercond Nov. Magn. **25** (2012) 785–789. https://doi.org/10.1007/s10948-011-1339-6**.**

[60] T. Hwa, P. Le Doussal, D. R. Nelson, and V. M. Vinokur, Flux pinning and forced vortex entanglement by splayed columnar defects, Phys. Rev. Lett. 71(1993) 3545. https://doi.org/10.1103/PhysRevLett.71.3545

[61] E. Bayazit, S. Altin, M.E. Yakinci, M.A. Aksan, Y. Balci, The effect of Mo addition on the microstructure and J_c properties of MgB_2 tapes fabricated by PIT method, J. Alloys Comp. 457 (2008) 42–46.

[62] E.S. Nurbaisyatul, H. Azhan, K. Azman, N. Ibrahim, Effect of CeO_2 Nanoparticle on the Structural and Electrical Properties of BSCCO-2223 High Temperature Superconductor, Solid State Phenomena 307 (2019) 104-109. doi:10.4028/www.scientific.net/SSP.307.104

[63] H. Azhana, J. S. Hawa, C. M. N. Azura, K. Azman, S. A. Syamsyir , Structural and electrical properties of high and low-density yb-doped Bi(Pb)-2223 superconductor, Jurnal Teknologi 78 (2016) 7-12. 10.11113/jt.v78.9014

[64] A.I. Abou Aly, I.H. Ibrahim, R. Awad, et al., Stabilization of Tl-1223 phase by arsenic substitution, J Supercond. Nov. Magn. 23 (2010) 1325–1332.

[65] J.H. Koo, G. Cho, The spin-gap in high T_{-c} superconductivity, J Phys: Condens. Matter. 15 (2003) L729–L733.

[66] W. Abdeen, S. Marahba, R. Awad, A.I. Abou Aly, I.H. Ibrahim, M. Matar, Journal of Advanced Ceramics 5(1) (2016) 54–69.

[67] M. Konczykowski, S. Colson, C.J. van der Beek, M.V. Indenbom, P.H. Kes, E. Zeldov, Magnetic relaxation in the vicinity of second magnetization peak in BSCCO crystals, Physica C 332 (2000) 219–224.

[68] M.I. Dolz, Y. Fasano, H. Pastoriza, V. Mosser, M. Li, M. Konczykowski, Latent-heat and non-linear vortex liquid at the vicinity of the first-order phase transition in layered high-T_c superconductors, Physical Review B 90 (2014) 144507

[69] V.M. Vinokur, B. Khaykovich, E. Zeldov, M. Konczykowski, R.A. Doyle, P.H. Kes, Physica C 295 (1998) Ž . 209.

[70] S. Eley, R. Willa, M.K. Chan, *et al.* Vortex phases and glassy dynamics in the highly anisotropic superconductor $HgBa_2CuO_{4+\delta}$. *Sci Rep* 10 (2020) 10239. https://doi.org/10.1038/s41598-020-65224-5.

[71]Burlachkov, L., Geshkenbein, V. B., Koshelev, A. E., Larkin, A. I. & Vinokur, V. M. Giant flux creep through surface barriers and the irreversibility line in high-temperature superconductors. *Phys. Rev. B* 50 (1994) 16770.

[72]Burlachkov, L. Magnetic relaxation over the Bean-Livingston surface barrier. *Phys. Rev. B* 47(1993) 8056–8064.

[73] C.P. Bean, Magnetization of Hard Superconductors, Phys. Rev. Lett. 8 (1962) 250-253.

[74]O. Bilgili, K. Kocabaş, Effect of Nb addition on magnetic, structural and superconducting properties of (Bi, Pb)-2223 superconductors, J. Mater. Sci. Mater. Electron. 25 (2014) 2889. https://doi.org/10.1007/s10854-014-1956-5

[75] M. E. Aytekin, B. Özkurt, The Influence of Nano-Sized SnO_2 Doping on Physical and Magnetic Properties of the $Bi_2Sr_{2-x}(SnO_2)_xCa_1Cu_{1.75}Na_{0.25}O_y$ Superconductors, J. Supercond. Nov. Magn. 33 (2020) 965–970. https://doi.org/10.1007/s10948-019-05336-w.

[76] K.-H. Muller, C. Andrikidis, J. Du, K.E. Leslie, C.P. Foley, Connectivity and limitation of critical current in Bi-Pb-Sr-Ca-Cu/Ag tapesPhys. Rev. B. 60 (1999)659. https://doi.org/10.1103/PhysRevB.60.659.

[77]T. Tokuda, K. Hidaka, S. Kishida, Superconducting characterization of Ni/$Bi_2Sr_2Ca_2Cu_3O_y$ superconductors, Physica C. 464-465 (2007) 942. https: //doi. org/10.1016/j.physc.2007.04.277

[78] N. Sivakumar, A. Narayanasamy, K. Shinoda, C.N. Chinnasamy, B. Jeyavedan, J.M. Greneche, Electrical and magnetic properties of chemically derived nanocrystalline cobalt ferrite,J. Appl. Phys. 102 (2007) 013916. https://doi.org/10.1063/1.2752098

[79] B.A. Albiss , I.M. Obaidat , M. Gharaibeh , H. Ghamlouche, S.M. Obeidat, Impact of addition of magnetic nanoparticles on vortex pinning and microstructure properties of Bi–Sr–Ca–Cu–O superconductor, Solid State Communications 150 (2010) 1542-1547. https://doi.org/10.1016/j.ssc.2010.06.001.

[80] V. Sandu, Pinning-force scaling and its limitation in intermediate and high temperature superconductors, Mod. Phys. Lett. B. 26 (2012) 1230007. https: //doi. org/ 10.1142/S0217984912300074.

[81] A. Los, B. Dabrowski, K. Rogack, Increase of $YBa_2Cu_3O_7$ critical currents by Mo substitution and high-pressure oxygen annealing, Current Applied Physics,27 (2021),1-6,https://doi.org/10.1016/j.cap.2021.03.007.

[82] J. Rochester, M. Ortino, X. Xu, X. Peng and M. Sumption, The Roles of Grain Boundary Refinement and Nano-Precipitates in Flux Pinning of APC Nb3Sn, *IEEE Transactions on Applied Superconductivity*, 31 (2021) 1-5, Art no. 8000205, doi: 10.1109/TASC.2021.3057560.

[83] D. Sharma, R. Kumar, V.P.S. Awana, DC and AC susceptibility study of sol–gel synthesized $Bi_2Sr_2CaCu_2O_{8+d}$ superconductor, Ceram. Int. 39 (2013) 1143–1152, https://doi.org/10.1016/j. sacrament.2012.07.038.

[84] A. A. El Hassan, A. Labrag, M. Bghour, A. Taoufik, Determination of the critical current density and the flux pinning force in single crystals $YBa_2Cu_3O_{7-\delta}$ from the magnetization hysteresis cycles, Chinese Journal of Physics (2020), https://doi.org/10.1016/j.cjph.2020.06.025

[85]F.Buta, M.Bonura, D.Matera, G. Bovone, A. Ballarino, S.C. Hopkins, B. Bordini, X. Chaud, C. Senatore, Very high upper critical fields and enhanced critical current densities in Nb_3Sn superconductors based on Nb–Ta–Zr alloys and internal oxidation, Journal of Physics: Materials 4:2 (2021) 025003.

[86]A. Biju, U. Syamaprasad, S. Vinu, R. Shabna, P.M. Sarun, Enhancement of flux pinning and Anderson–Dew-Hughes pinning analysis in $Bi_{1.6}Pb_{0.5}Sr_{2-x}Tb_xCa_{1.1}Cu_{2.1}O_{8+\delta}$ superconductor, J. Alloy. Comp. 477 (2008) L13–L16, https://doi.org/10.1016 /j.jallcom.2008.10.033

List of Figures:-

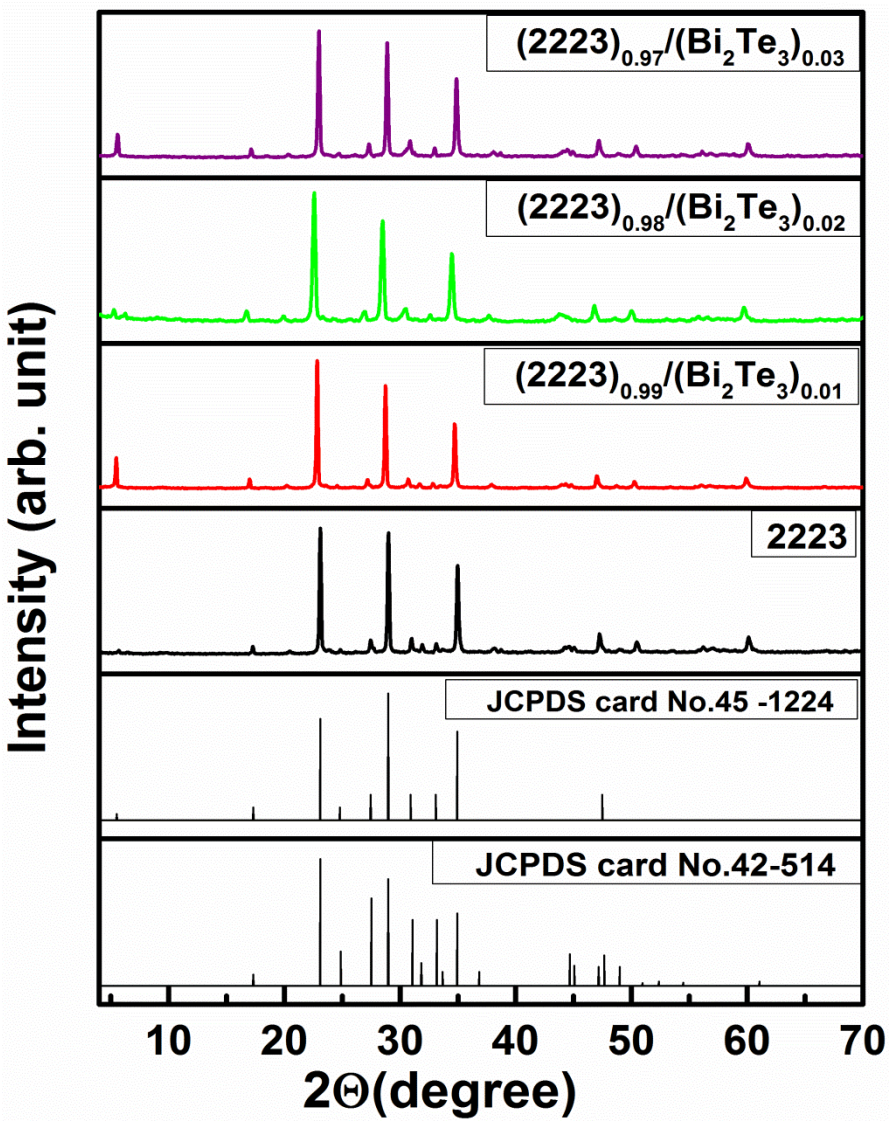

Figure (1): X-ray diffractogrames at room temperature for the system $(Bi_{1.6}Pb_{0.4}Sr_2Ca_2Cu_{3-y}O_{10+\delta})_{1-x}/(Bi_2Te_3)_x$ with (x=0.00,0.01,0.02,0.03) and simulated JCPDS cards.

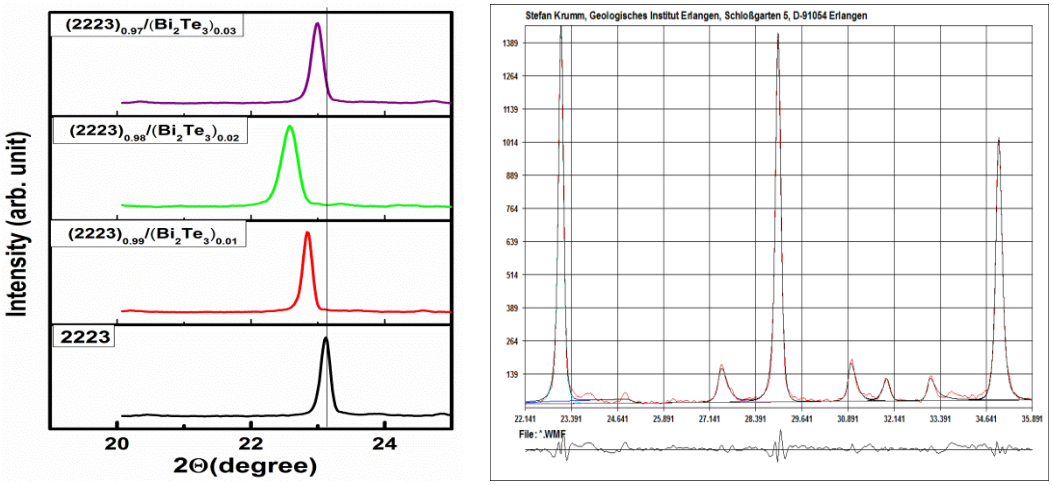

Figure (2): a) The peak shift of the strongest peak due to the Bi_2Te_3 doping, b) the deconvolution analysis using Winfit program for the strongest lines of BSCCO sample.

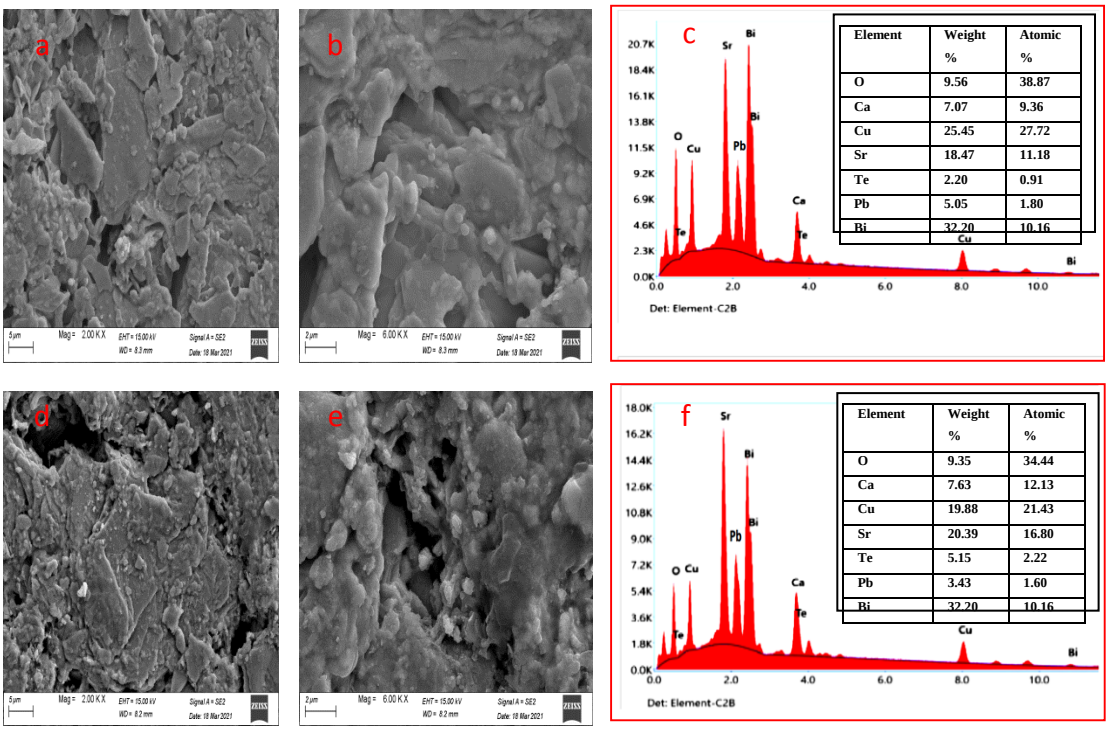

Element	Weight %	Atomic %
O	9.56	38.87
Ca	7.07	9.36
Cu	25.45	27.72
Sr	18.47	11.18
Te	2.20	0.91
Pb	5.05	1.80
Bi	32.20	10.16

Element	Weight %	Atomic %
O	9.35	34.44
Ca	7.63	12.13
Cu	19.88	21.43
Sr	20.39	16.80
Te	5.15	2.22
Pb	3.43	1.60
Bi	32.20	10.16

Figure (3): SEM analysis of pellets samples with different magnifications :- (a &b) SEM images, and (c) EDX spectrum of $(Bi_{1.6}Pb_{0.4}Sr_2Ca_2Cu_{3-y}O_{10+\delta})_{0.99}/(Bi_2Te_3)_{0.01}$ sample where (d &e) SEM images and (f) EDX spectrum of $(Bi_{1.6}Pb_{0.4}Sr_2Ca_2Cu_{3-y}O_{10+\delta})_{0.97}/(Bi_2Te_3)_{0.03}$ sample, respectively.

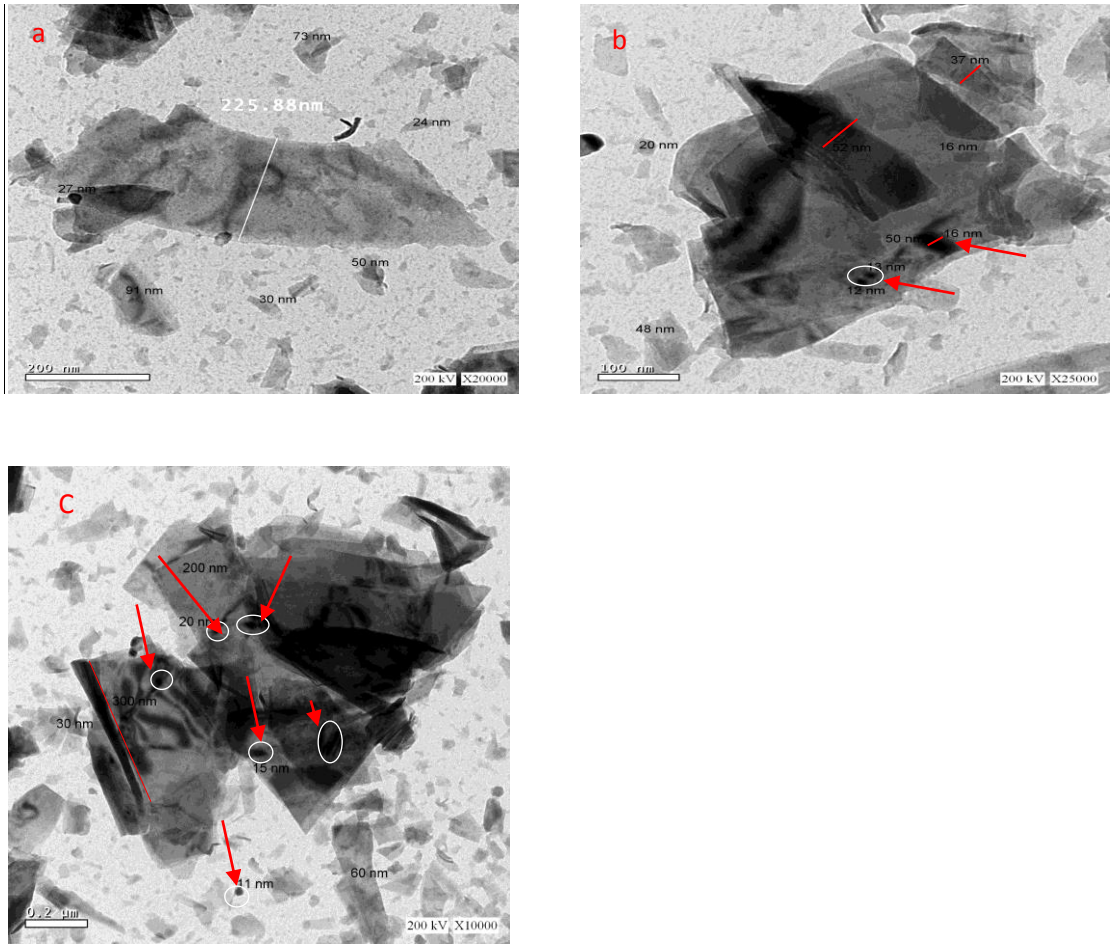

Figure (4): TEM images of $(Bi_{1.6}Pb_{0.4}Sr_2Ca_2Cu_{3-y}O_{10+\delta})_{0.99}/(Bi_2Te_3)_{0.01}$ sample.

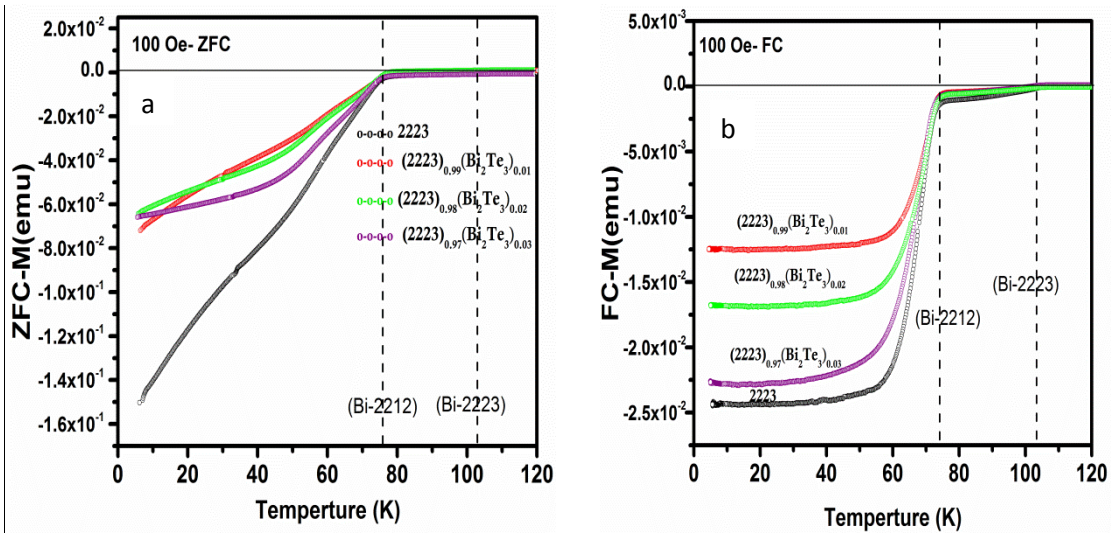

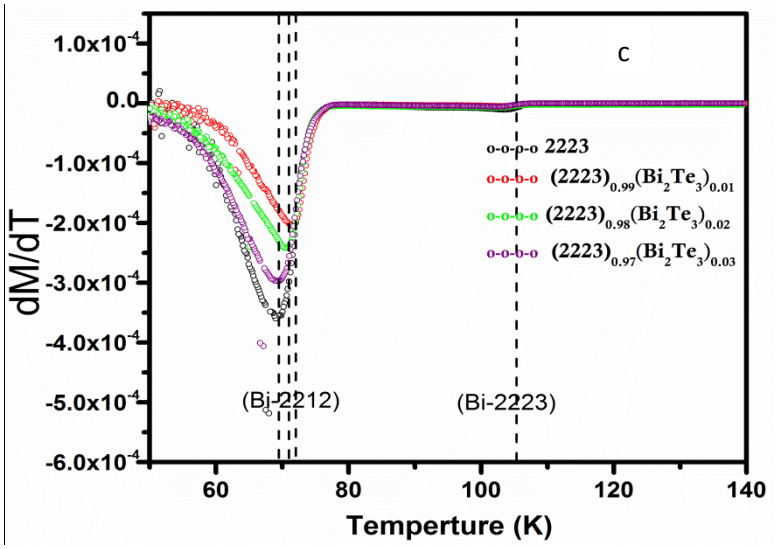

Figure (5): Magnetization versus temperature M(T) dc magnetization curves for $(Bi_{1.6}Pb_{0.4}Sr_2Ca_2Cu_{3-y}O_{10+\delta})_{1-x}/(Bi_2Te_3)_x$ with (x=0.00,0.01,0.02,0.03) samples: a) Zero field cooled (ZFC), b) Field cooled (FC) and c) dM/dT versus temperature curves calculated from (FC), respectively.

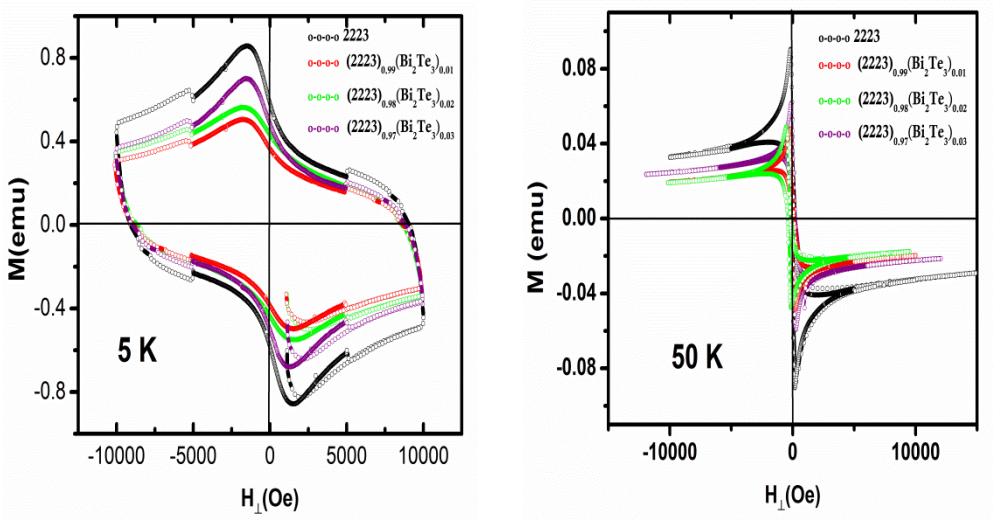

Figure (6): Typically (M–H) hysteresis loops for pure and 2223containing Bi_2Te_3 superconductor evaluated at T = 5 K & 50 K, respectively, between 0 and ±15 KOe.

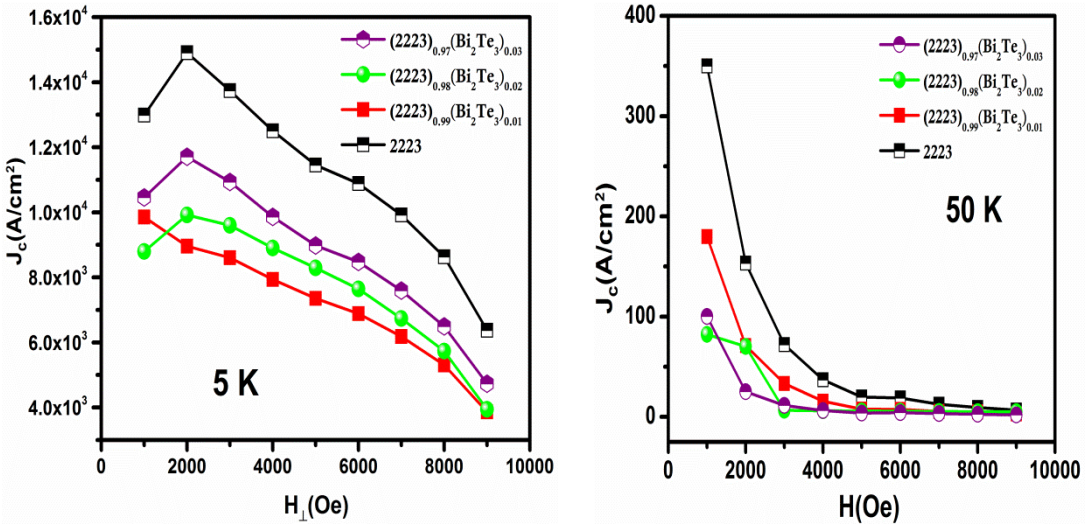

Figure (7): Typical plots of the critical current density (J_c) as a function of H for 2223 and 2223 containing various amounts of Bi_2Te_3 at T = 5 K and 50 K, respectively.

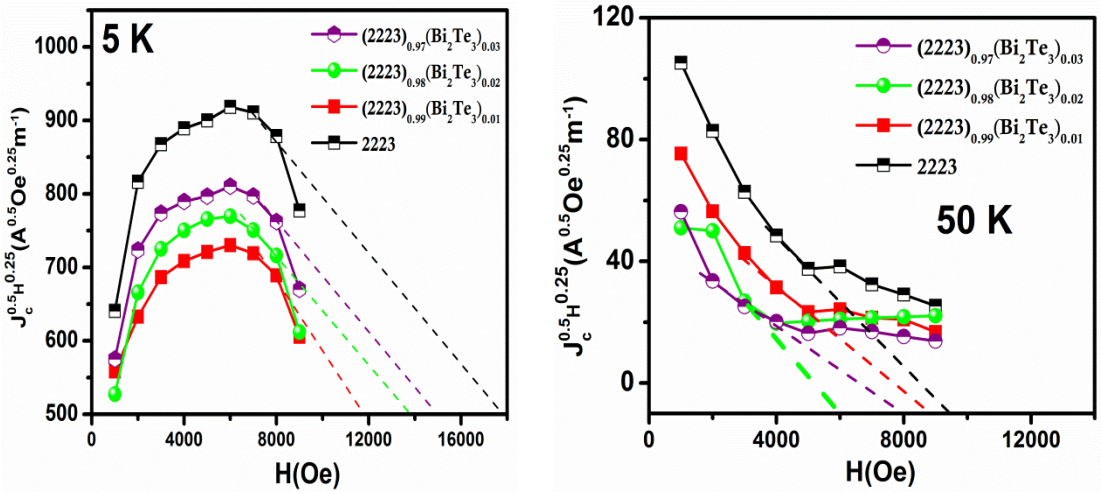

Figure (8): Plots of a schematic representation of $Jc^{0.5}$ $H^{0.25}$ as a function of H to determine the irreversible filed (H_{irr}) of 2223 and 2223 containing various amounts of Bi_2Te_3 wt.% at T = 5 &50 K, respectively.

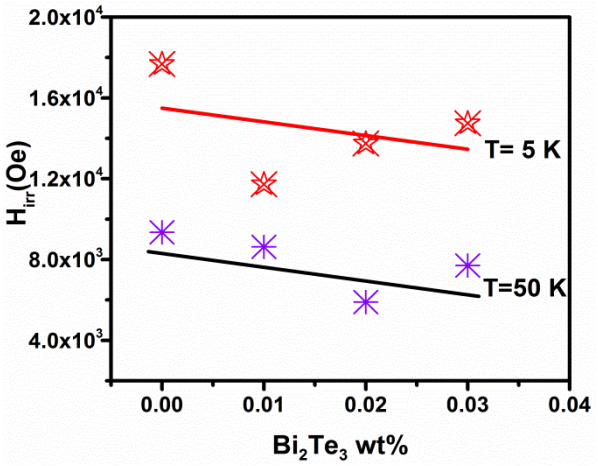

Figure (9): Irreversible filed (H_{irr}) for 2223 and 2223 containing various amounts of Bi_2Te_3 wt.% pellets plotted as a function of Bi_2Te_3 wt.% at T = 5 &50 K, respectively. A solid line demonstrates the linear fit of H_{irr} data.

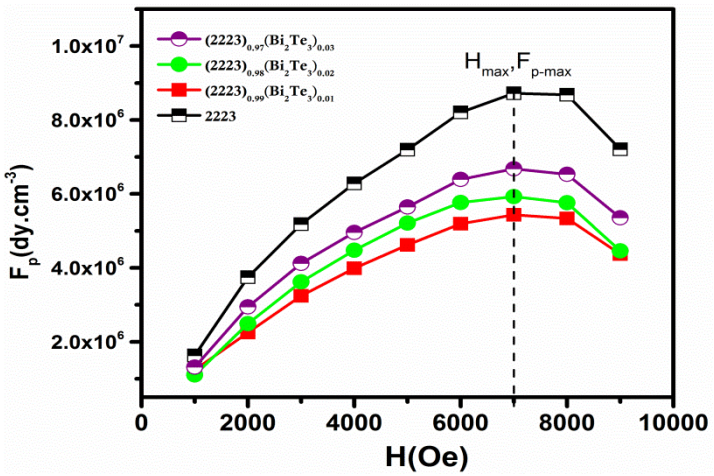

Figure (10): Magnetic field dependencies of F_p for 2223 and 2223 containing various amounts of Bi_2Te_3 wt. % pellets at T = 5 K.

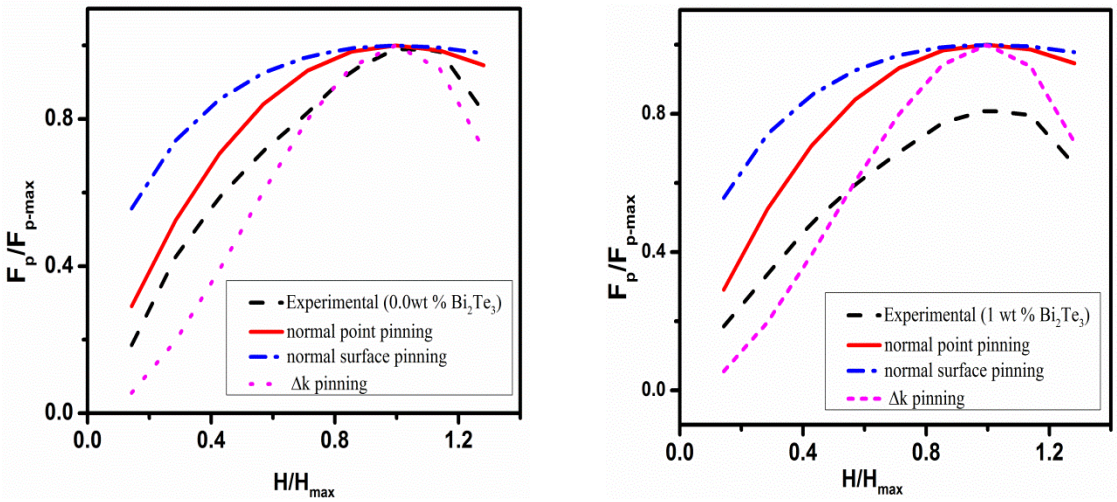

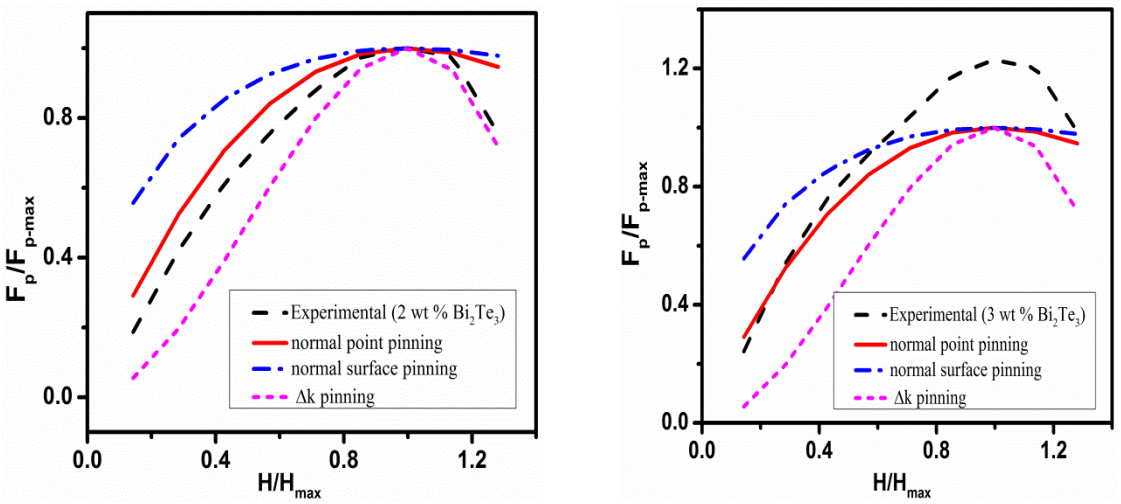

Figure (11): Normalized pinning force vs. the normalized magnetic field with various Bi_2Te_3 wt. % at 5 K. Doted (Magenta), solid (red), and dashed (blue) lines signify the theoretical plots based on Eqs. (2)–(4) respectively.

List of Tables:-

Table (1): Volume fractions and lattice parameters (± standard deviation (σ)) of the identified phases in $(Bi_{1.6}Pb_{0.4}Sr_2Ca_2Cu_{3-y}O_{10+\delta})_{1-x}/(Bi_2Te_3)_x$ with (x=0.00,0.01,0.02,0.03) samples.

Sample	Phase	Volume fraction	Lattice parameters (Å)			Unit cell volume (Å^3)	Grain size (nm)	Strain X 10^{-3}	T_{c1} (K)	T_{c2} (K)
			a	b	c					
2223	Bi-2223	51	5.40±0.0131	5.39±0.0461	30.83±0.0131	899.21±2.3347	92	2.22	107	69.5
	Bi-2213	49	5.40±0.0158	5.48±0.0265	30.87±0.0586	916.01±3.7747				
$(2223)_{0.99}/(Bi_2Te_3)_{0.01}$	Bi-2223	55	5.45±0.0169	5.48±0.0608	30.98±0.0452	926.56±2.8048	99	2.25	104	69.5
	Bi-2213	45	5.40±0.0241	5.50±0.0407	30.84±0.0891	918.61±1.7978				
$(2223)_{0.98}/(Bi_2Te_3)_{0.02}$	Bi-2223	52	5.49±0.0330	5.57±0.092	31.19±0.0880	955.62±6.8766	38	6.52	105	70.6
	Bi-2213	48	5.40±0.0485	5.45±0.0833	30.97±0.1809	927.95±4.8893				
$(2223)_{0.97}/(Bi_2Te_3)_{0.03}$	Bi-2223	52	5.42±0.0096	5.45±0.0344	30.86±0.0256	913.77±3.4969	70	2.84	102	71.7
	Bi-2213	48	5.40±0.0173	5.46±0.0285	30.88±0.0639	911.87±2.732				

Ms. Ref. No.: CERI-D-21-02347R1
Title: The impact of the addition of Bi_2Te_3 nanoparticles on the structural and the magnetic properties of the Bi-2223 high-Tc superconductor.
Ceramics International

Dear Editor for Ceramics International Journal.

We thank you and the referees for very useful comments, we have accounted for all comments by all referees to improve the manuscript and hope that you now find the revised version acceptable for publication in *Ceramics International*.

Below we quote each comment made by the referees in normal font followed by our responses in blue font. We have revised and modified the corrections inside our manuscript in yellow color (3rd reviewer) highlight.

Comments made by the referees are listed below (point by point):

Reviewer's comments:

Reviewer 3: • The author's response to "In experimental part, authors have used very high temperature value (860 C which is very close to sintering temperature) for the calcination process. Why they have used such a high temperature? Normally, 750-800 C is used for the calcination and at the temperature they used, almost superconducting phases start to forming" is not satisfactory. Because, in the calcination process, it is aimed to decompose the alkaline-earth carbonates, not to increase the volume fraction of Bi-2223 phase without any secondary impurities.

Author's comment: Yes, We know that Bi-2223 phase formation strongly depends on the preparation conditions such as sintering temperature, thermal processing time, synthesis atmosphere, precursor compositions. Here we used such a high temperature 860 C was trying to take the risk to check the effect of this temperature on the materials. Then we went through the steps and finally made the measurements, first by the XRD to check the phases. We found that the usage conditions give us the XRD pattern without impurities; just the typical phases of Bi-2212 and Bi-2223 existed. Unfortunately, we do not achieve a single phase for the prepared samples.

• The author's response to "For the pure sample the authors have used 870 C but for the others (added nanoparticles) they have used 850C. why? Have they measured DSC/TGA in order to obtain the melting and crystallization temperatures? If they have not measured it will not be sense to compare the results since the experimental conditions are not the same" is not satisfactory. Because the preparation conditions are not the same. So-called dark materials have been sintered at 870 C for 48 hours, but the powders including Bi2Te3 were sintered at 850 C. Therefore, it can be more logical and scientifical approach, if the preparation conditions would be same.

Author's comment: We studied the addition of Bi2Te3 nanoparticles on Bi-2223, so we do the preparation process until the phase formation as studied before in many papers (they prepare BSCCO). They add the nanoparticle compounds in the final

stage [1,2,3,4]). In the final stage, we divide the material into four parts (one blank without any additive (pure) and three with Bi2Te3 addition). The four samples (the blank (pure), without any additive) and the three additive samples were exposed to the final stage of sintering).
The comparison has been made between the pure BSCCO and the additive BSCCO after the samples were exposed to the same process (in our case, the final stage).
If we make doping or substitution with elements, we will use its oxide with the starting materials, but here we want to examine the effect of the additive of Bi2Te2 on BSCCO.
I highlighted and rewrote this again in the experimental part.

The authors make same process:

1-B.A. Albiss , I.M. Obaidat , M. Gharaibeh , H. Ghamlouche, S.M. Obeidat, Impact of addition of magnetic nanoparticles on vortex pinning and microstructure properties of Bi-Sr-Ca-Cu-O superconductor, Solid State Communications 150 (2010) 1542-1547

2- H. Baqiah, S.A.Halim, M.I.Adam, S.K.Chen, S.S.H.Ravandi, M.A.M.Faisal, M.M.Kamarulzaman and M.Hanif "THE EFFECT OF MAGNETIC NANOPARTICLE ADDITION ON THE SUPERCONDUCTING PROPERTIES OF $Bi_{1.6}Pb_{0.4}Sr_2Ca_2Cu_3O_\delta$ SUPERCONDUCTORS", Solid State Science and Technology, Vol. 17, No 1 (2009) 81-88.

3- M. Roumié, S. Marhaba, R. Awad, M. Kork,I. Hassan, R. Mawassi, " Effect of Fe_2O_3 Nano-Oxide Addition on the Superconducting Properties of the (Bi,Pb)-2223 Phase", J Supercond Nov Magn (2014) 27:143–153 DOI 10.1007/s10948-013-2288-z

4- N. Boussouf · M.-F. Mosbah," Effects of BCO_3 Addition on the Formation and Properties of the Bi-Based Superconductors", J Supercond Nov Magn (2013) 26:2891–2897 DOI 10.1007/s10948-012-2091-2

All of them prepare the material first and then add the nano-compounds at the final stage.

- The author's response to "Fig.2 includes the XRD patterns of non-added and Bi2Te3 nano-particles added in Bi-2223 superconductors. The general behavior of XRD patterns shows the same characters, i.e. pointing all the samples have same character and no difference in their crystal properties. But still there are several peaks as undefined. In addition, the y-scale was labeled with the numbers but intensities are still in arbitrary unit" is not satisfactory. It will be more understandable if the authors normalized to y-axis by using the formula given below:

x (the normalised value) =[a(the intensity value)–amin (the minimum value obtained in the intensity)]/[amax (the maximum value obtained in the intensity)–amin]]

Reference: C. Kaya, B. Özçelik, B. Özkurt, A. Sotelo, M. A. Madre
"Effect of Ce substitution on structural and superconducting properties of Bi-2212 system"
J Mater Sci: Mater Electron (2013) 24:1580–1586 DOI 10.1007/s10854-012-0979-z

Author's comment: The formula was used as your demand, Figure 1 and 2 (XRD figures) were modulated according to the normalization formula (highlighted with yellow), and the paper was cited with reference no.[49].